

# Low-Cost and High-Speed Fabrication of Camouflage-Enabling Microfluidic Devices using Ultrahigh Molecular Weight Polyethylene

Xiaoruo Sun, Asad Asad,\* Mehnab Ali, Luka Morita, Patricia I. Dolez, James D. Hogan, and Dan Sameoto\*

This study demonstrates a multi-spectrum camouflage control via microfluidic methods within a thermally and visibly semi-transparent polymer (polyethylene). Microfluidic devices have a high potential for achieving multiband camouflage including both visible and infrared (IR) spectrums because they can manipulate fluids that may be dyed, transparent, or opaque to different parts of the electromagnetic spectrum. However, most traditional polymers used for microfluidics are not very transparent in the thermal IR region ( $\approx 8\text{--}14\text{ }\mu\text{m}$  wavelengths), which limits their effectiveness in this spectrum. It develops a high-speed, low-cost robust process to fabricate microfluidic devices entirely made from polyethylene using xurography and thermocompression molding techniques. Moreover, a novel method that thermally bond macro-scale polyethylene tubing to micro-scale channels is developed. The simplicity and flexibility of the method allow the fabrication of devices with different channel heights, widths, and patterns. Upon filling the microfluidic devices with dyed liquids and testing them with different backgrounds, the devices show fast and high visible camouflage capabilities. Moreover, the thermal IR appearance of microfluidic systems can be altered without changing temperature by incorporating a metalized surface which can be covered by an IR opaque liquid to alter the apparent temperature when reflecting IR sources.

## 1. Introduction


Microfluidic devices and related technologies have been widely studied, researched, and fabricated for decades.<sup>[1–3]</sup> The history of research and fabrication of microfluidic devices dates back to the late 1970s;<sup>[4,5]</sup> However, the progress in the early stages of microfluidics was restricted by materials (silicon was used as a basic material early on) and fabrication techniques (photolithography, micromachining, and thin-film techniques).<sup>[6]</sup> Despite these limitations, modern microfluidic technologies were developed in the early 1990s.<sup>[3,7,8]</sup> Since then, the microfluidics field has experienced substantial growth and diverged into various areas including biochemical, biomedical, and optical areas.<sup>[9–11]</sup>

Camouflage is a crucial topic in the field of optics, as it provides a means of hiding from danger. Some animals show camouflage skills in nature by evolving a range of defensive color patterns including fixed and adaptive body coloration.<sup>[12,13]</sup> The limitation of fixed body coloration in an animal is evident as the color cannot adapt to the changing

background while in motion.<sup>[14]</sup> In contrast, cephalopods possess a remarkable ability to achieve rapid adaptive camouflage by altering their visual appearance in a matter of seconds.<sup>[15]</sup> Similarly, camouflage plays a crucial role in military operations, making it harder for soldiers to be detected or recognized.<sup>[16,17]</sup> The patterns of modern military camouflage are often designed digitally<sup>[18,19]</sup> with a fixed coloration pattern. Since the patterns are unchangeable, soldiers face difficulty in adapting to different environments or unpredictable situations.<sup>[20,21]</sup> Researchers have been investigating innovative methods of adaptive camouflage utilizing microfluidic technology.<sup>[22]</sup> In this approach, a colored liquid fills a specific microfluidic pattern, which can rapidly alter its appearance to blend in with the surrounding environment. A type of liquid color-changing lens with a microfluidic channel was developed with the capability of vision protection, camouflage, and optical filtering.<sup>[23]</sup> However, the material used was poly(dimethylsiloxane) (PDMS), which is not IR transparent

X. Sun, A. Asad, M. Ali, L. Morita, J. D. Hogan, D. Sameoto  
Department of Mechanical Engineering  
University of Alberta  
Edmonton T6G 2G8, Canada  
E-mail: aaasad@ualberta.ca; sameoto@ualberta.ca

P. I. Dolez  
Department of Human Ecology  
University of Alberta  
Edmonton T6G 2N1, Canada

 The ORCID identification number(s) for the author(s) of this article can be found under <https://doi.org/10.1002/admt.202300705>

© 2023 The Authors. Advanced Materials Technologies published by Wiley-VCH GmbH. This is an open access article under the terms of the Creative Commons Attribution-NonCommercial License, which permits use, distribution and reproduction in any medium, provided the original work is properly cited and is not used for commercial purposes.

DOI: 10.1002/admt.202300705

and, thus, limited its application for visible camouflage. To the author's knowledge, only one microfluidic device that used PE was fabricated to manipulate both visible and infrared appearance. This device was fabricated using levels of channels combined with thermocompression molding.<sup>[24]</sup> Although the device achieved the proposed goal, the mold manufacturing required chemical etching of a stainless-steel sheet that adds extra complexity to the device's fabrication. Moreover, many of the chemical etchants are highly corrosive, toxic, and pose a risk to human health and the environment.<sup>[22,24–25]</sup>

Microfluidic devices capable of achieving color-changing camouflage followed specific critical design and fabrication rules for material selection. In particular, only visible transparent or semitransparent materials should be used as the surface (top) layer of these devices to enable the efficient manipulation of fluids and enable the desired color-changing effects.<sup>[24–26]</sup> Most microfluidic materials have been used to fabricate transparent microfluidic devices in the visible spectrum. Silicon was used for the very first devices.<sup>[4,5]</sup> Ecoflex silicone rubber was used for a soft robot with microfluidic channels to create a camouflage system.<sup>[25]</sup> Silica gel can also be used to fabricate microfluidic devices.<sup>[27]</sup> In addition, PDMS is a mineral-organic polymer (a structure containing carbon and silicon) that has been one of the most actively developed and foundational polymers for microfluidics.<sup>[23,28–33]</sup> Thermoplastic polymer materials such as poly(methyl methacrylate) (PMMA), polycyclic olefin (PCO), polycarbonate (PC), and polystyrene (PS) can also be alternative materials to fabricate color-changing microfluidic devices as they are optically transparent.<sup>[34]</sup> However, these different materials are opaque to infrared light. On the other hand, Polyethylene (PE) is transparent from the visible region to the end of mid-IR,<sup>[24,31]</sup> which makes it a promising candidate for combined visible and IR camouflage.

The selection of fabrication methods for camouflage microfluidic devices is restricted by the need to ensure both simplicity and reliability while maintaining optical transparency and precise control over the microchannel geometry.<sup>[35,36]</sup> The traditional microfluidic device fabrication methods can be classified into two main categories, material removal techniques (subtractive) and material depositing techniques (additive). However, material deposition usually requires the material can be applied in desired amounts at specific locations; the material needs to be transportable and can turn into a solid at that location.<sup>[37]</sup> On the other hand, material removal techniques have fewer requirements regarding material properties; therefore, removal techniques have been more generally applied.<sup>[37]</sup> Besides this classification in terms of material addition and removal, the fabrication methods can also be identified by the processes, including chemical processes, mechanical processes, and laser-based processes. More information can be found in detailed reviews published on these fabrication processes.<sup>[3,37,38]</sup> Some processes are complex with multiple steps/operations involved (such as chemical etching); some of them such as laser-based processes are expensive; some of them such as electrochemical discharge machining can only be performed in a cleanroom facility; and many of them can suffer weak reproducibility, low resolution, material restriction, and slow rates.<sup>[3,38]</sup> However, there is one mechanical process for material removal that is low-cost and fast and does not need to be performed in a cleanroom facility.<sup>[3,39]</sup>

Xurography, which is also known as razor writing, is an environmentally friendly and flexible process that uses a cutter to pattern features in a material. Xurography also has the ability to fabricate inexpensive and robust microfluidic devices in a short time.<sup>[40,41]</sup>

Besides channel manufacturing, it is also very important to connect the micro-structured device to the outer world, which is often referred to as the macro-to-micro interface. Since the interface between the microfluidic device and the peripherals (tubing) is typically the least reliable components of a microfluidic device, getting interconnection robust has a significant impact on the overall performance. Moreover, the processes used to integrate fluidic connections typically contribute to the overall cost of the device.<sup>[42,43]</sup> A review of works regarding microfluidic interfaces can be found in this document.<sup>[43]</sup>

In this study, we demonstrated a fast (few minutes) and inexpensive (less than 0.1 Canadian dollar per piece) fabrication technique for a multilayered microfluidic device with adaptive camouflage capabilities. It is featured with a microchannel structure and is based on a single material, ultrahigh molecular weight polyethylene (UHMWPE). This technique combines xurography (for the channel layer) and a thermal bonding process to complete the whole system. The process has the capability to be mass produced since the manufacturing can be standardized at scale by using punches or other cutting tools to produce complex channels from sheets. In addition, our fabrication technique shows the flexibility of the design as the size and aspect ratio of the microfluidic channel is fully tunable by different cutting patterns and choice of type of stock material. The microfluidic channel device demonstrates the ability to achieve visible camouflage by filling the channel with dyed liquids to match the microfluidic device to the background color as the device itself is semi-transparent and the transparency can be improved by simple surface treatment. In addition, the semi-IR transparent nature of polyethylene allows this design to also achieve IR camouflage by changing the IR appearance of an embedded metalized surface. The manufactured microfluidic devices were characterized in terms of the channel dimensions, IR & visible properties, and visible and IR camouflage effectiveness in matching different backgrounds.

## 2. Experimental Section

### 2.1. Materials

Ultrahigh molecular weight polyethylene film (UHMWPE, McMaster-Carr, Thickness = 0.004" and 0.01") and polyethylene tubing (PE tubing, McMaster-Carr, Inner Diameter = 1/16", Outer Diameter = 1/8") were utilized to fabricate the visible camouflage microfluidic channel device. Food dyes (E-Kongton, China) were used to prepare aqueous dyed solutions using deionized (DI) water. The concentration of the food dye in DI water was 20% weight ratio. An ultra-thin multi-layered metalized (aluminium) polyethylene sheet used in food packaging (Cleaned Cheetos Bugles Package Bag) was added to the original visible camouflage microfluidic device to obtain an IR camouflage device. DI water was used as the circulation fluid inside the channel. All the materials were used without modifications and can be considered commercial off-the-shelf (COTS) components.

## 2.2. Equipment

A craft cutter (Silhouette Cameo 4, China) was used to fabricate the microchannel layer. The cutting pattern could be designed either by the Cameo 4 studio software or the drawing file could be imported from an engineering drawing software (SolidWorks was used for the design). The heat bonding of the layers of the microfluidic device was performed with a hot plate (HS40A Scientific Programmable and Stirring Hot Plate, Torrey Pines, USA) and a T-shirt heat press. A setup with a syringe was developed to circulate the liquid within the microfluidic channel. An oven (Isotemp™ Model 281A Vacuum Oven, Fisherbrand™, USA) was used as a thermal background for the infrared transparency demonstration. A 3D printer (Ender 3, Creality 3D, China) heating bed was used as a thermal source for the infrared reflection characterization. The cross-section of the microfluidic channels was analyzed using a Field Emission Scanning Electron Microscope (FE-SEM, Zeiss, Oberkochen, Germany). The infrared and visible spectra of the microfluidic devices were measured using attenuated total reflectance Fourier transform infrared (ATR-FTIR, Agilent Cary 600 series, Canada) and UV-vis spectrophotometer (Thermo Fisher Scientific GENESYS™ 10, Canada), respectively. The pictures and videos of the microfluidic devices were recorded by smartphone (iPhone 13 Pro Max, USA).

## 2.3. Preparation of the Microchannel Layer

The microchannel layer was prepared by cutting a thin sheet of 0.004" UHMWPE with a blade using the craft cutter. In this design, the height of the microfluidic channels was mainly controlled by the thickness of the PE sheets used for each layer. The UHMWPE sheet was attached to a sticky mat for the cutting operation. The cutting setting was optimized for each thickness of PE sheet in order to achieve the highest accuracy of cutting along with an acceptable speed. More information on the cutting settings could be found in Table S1 (Supporting Information) After cutting the UHMWPE sheet, the layer was transferred to a piece of double-sided polyester tape (Flexmount DF051521). By removing the interior cut portion from the tape, the channel structure was achieved.

## 2.4. Fabrication of the Microfluidic Device for Visible Camouflage

The fabrication process of the visible camouflage microfluidic device was based on thermal bonding as shown in **Figure 1**. The order in which the layers were bonded matters as the microfluidic channel must have at least one inlet and one outlet for the connection tubes. The overall fabrication process consisted of three parts: the formation of the bottom layer (Figure 1a–d), which had the channel structures; the formation of the top layer (Figure 1e–h), which had the inlet/outlet tubes; and the final assembly of the two layers (Figure 1i–j).

The formation of the bottom layer started by placing a polyester sheet (which acted as a high-temperature tolerant release layer) on a hotplate set at a temperature of 180 °C. An UHMWPE sheet was placed on top of the polyester sheet. A silicone roller was used to ensure complete melting of the UHMWPE sheet (Figure 1a).

Convenient for this process, UHMWPE barely flows in its molten state due to the high molecular weight and is more of a rubbery solid than liquid; therefore, it maintained its dimensions and relative tolerances despite being above its melting point. Thereafter, the microchannel structure (prepared in the previous section) was placed on top of the heated UHMWPE sheet and rolled a few times to ensure good bonding between the channels and the bottom layer—detectable once both surfaces looked transparent with no visible voids (Figure 1b,c). Since the double-sided tape had a higher heat resistance than the UHMWPE sheet, it did not melt during this step and was easily peeled off after cooling. A permanent bond was achieved between the channel structure and the bottom sheet, and the PE 2-layer assembly remained adhered to the polyester sheet (Figure 1d).

The formation of the top layer began in a similar way as for the bottom layer by placing a polyester sheet on the hotplate at 180 °C then rolling a UHMWPE sheet on top of it until complete melting (Figure 1e,f). For heat bonding the PE tubes to the UHMWPE sheet, an extra layer of polyester sheet was required: it had two holes cut using a hole puncher (Figure 1e,f). The distance between the holes was the same as the distance between the inlet and the outlet of the microfluidic channel; the diameter of the holes was slightly larger than the PE tube (by <1mm) to ensure that the tubes could go through the holes in the polyester sheet. This polyester sheet with holes was then placed on top of the PE sheet and rolled with the silicone roller to form a sandwich structure so that the UHMWPE sheet was in between the two polyester layers. Thereafter, two 1-inch-long PE tubes were inserted through the holes in the polyester sheet and press melted to the UHMWPE layer. The bonding time between the tube and the UHMWPE sheet was ≈5 s, which was enough to ensure complete bonding. The sandwiched UHMWPE with the tubes was cooled down and the bottom polyester layer was removed (Figure 1g). Finally, a needle was used to punch through the PE tube and the UHMWPE layer, forming the inlet/outlet holes (Figure 1h).

The final step was to melt the bottom layer with the top layer on the hotplate at 180 °C. The top layer (with the polyester sheet) was placed on the bottom layer with the two tubes aligned with the inlet and outlet positions in the microfluidic structure in the bottom layer (Figure 1i). A silicone roller was used to ensure a complete bonding between the layers. After removal from the hotplate and cooling down, the polyester layers were removed, which completed the fabrication of microfluidic device (Figure 1j). If the polyester support were not used in the fabrication process, large membranes over reservoirs and channels would frequently buckle and self-adhere in undesirable locations (See Figure S1, Supporting Information).

The effectiveness of the fabrication method was evaluated by fabricating microfluidic channels with different thicknesses and heights. The channels were categorized based on their width into W1 (0.5mm), W2 (1.0mm), and W3 (2.0mm), while the height of the channels was categorized into H1 (0.004 inches), H2 (0.008 inches), and H3 (0.012 inches). The channel height for W1, W2, and W3 was fixed at 0.004 inches. The channel widths for H1, H2, and H3 were fixed at 1.0mm. Channel heights of 0.008 inches, and 0.012 inches were achieved by thermally bonding two and three layers of the 0.004 inch thick sheets, respectively, prior to cutting the channels.

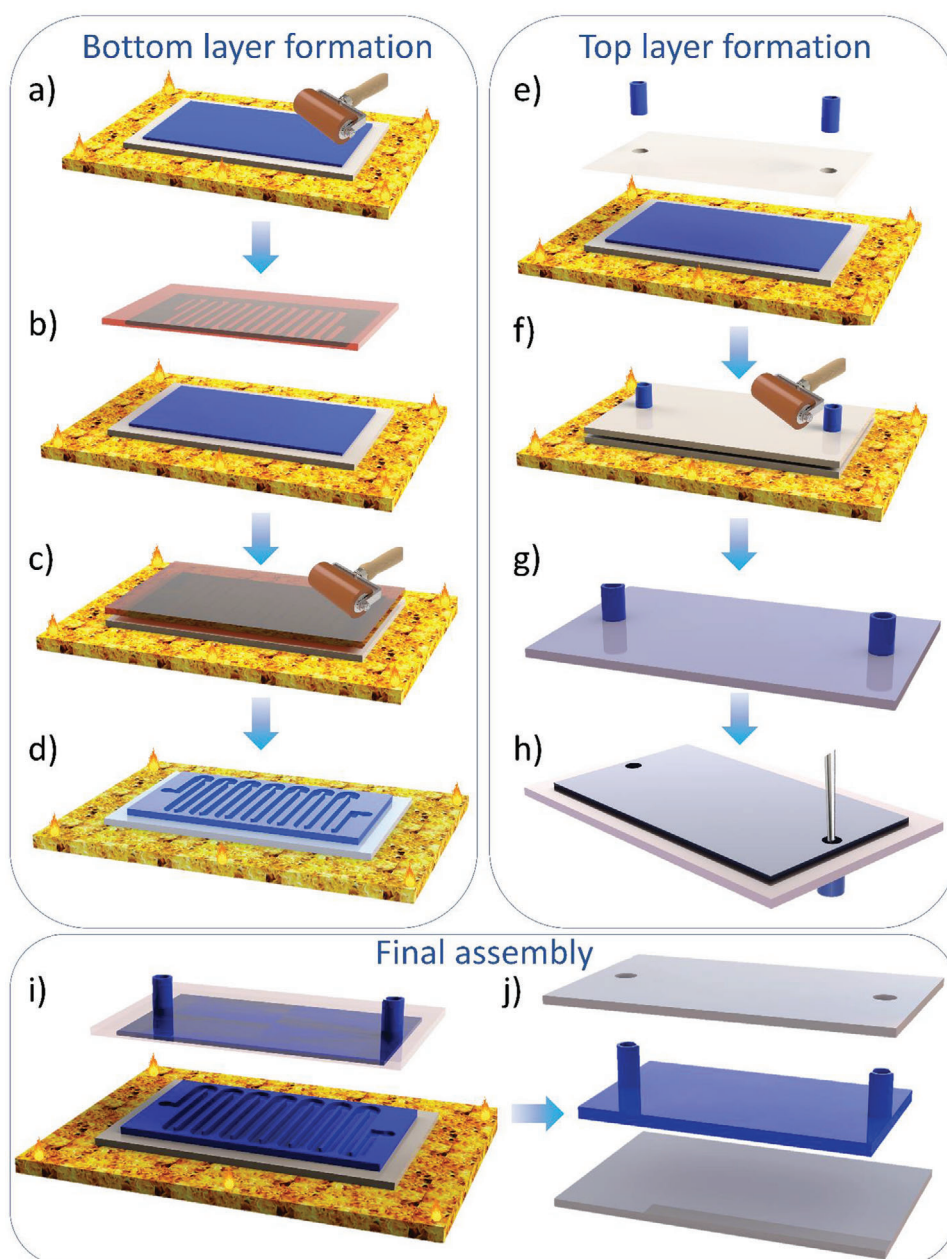


**Figure 1.** The fabrication steps of the microfluidic devices including the top layer, the bottom layer, and the final assembly: a) melting an UHMWPE sheet on a polyester substrate at 180 °C; b,c) bonding and rolling the taped UHMWPE layer with the microchannel structure on the melted UHMWPE sheet; d) peeling off the double-sided tape from the channels, which results in the formation of the bottom layer; e) melting and sandwiching an UHMWPE sheet between two polyester sheets with the top polyester layer having holes for the inlet/outlet tubes; f) melting PE tubes through the holes of the top polyester sheet to the sandwiched UHMWPE sheet and rolling the structure to ensure complete melting; g,h) removing the bottom polyester and piercing holes through the PE tubes to form the inlet/outlet channels; i,j) melting the top and bottom layers to form the final microfluidic device.

## 2.5. Fabrication of the Microfluidic Device for IR Camouflage

The fabrication process of the IR camouflage microfluidic device was very similar to the visible one (Figure 1). The main difference is that the IR camouflage device uses an additional metalized layer between the microchannel layer and the bottom layer. This was achieved by embedding a metalized polyethylene laminate film from food packaging between a 0.004" UHMWPE

sheet and a 0.01" UHMWPE sheet (that served as a harder back layer to support the package bag) by using the T-shirt heat press set to 148.9 °C. The metal side was facing upward and placed in between two PE sheets; the 0.004" UHMWPE was used as the top layer, and the 0.01" UHMWPE was used as the bottom to form a sandwich structure. When bonded between two PE sheets, the package bag was flattened and kept mechanically stable for the following xurography process. For this operation, the



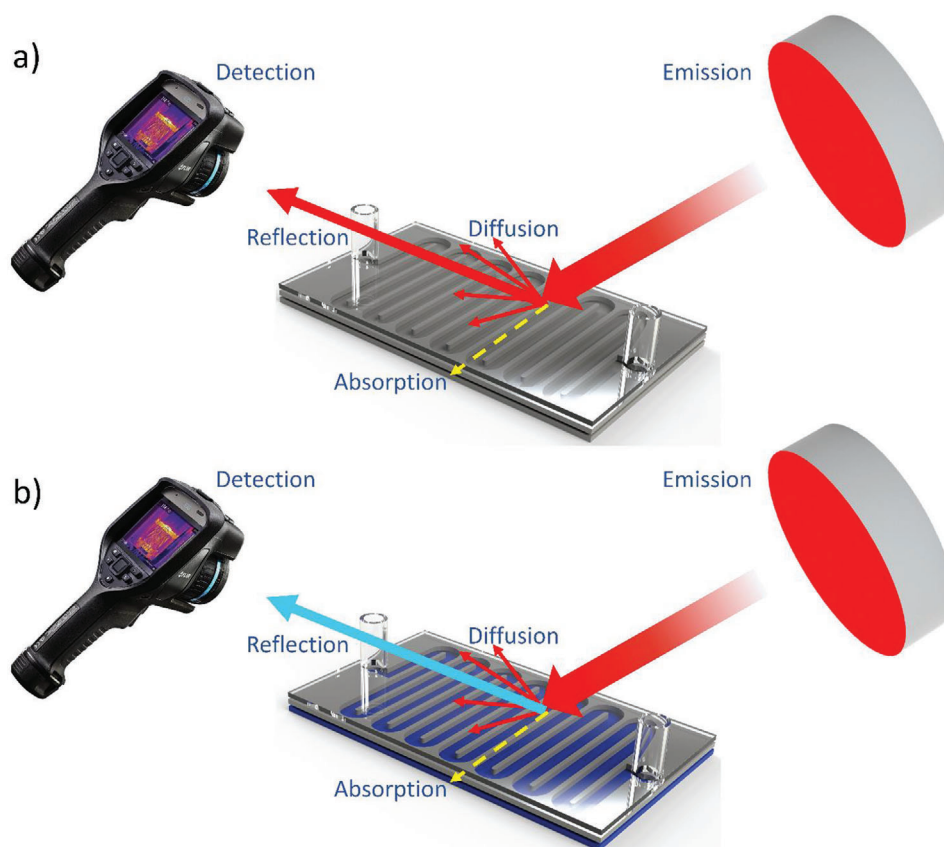


**Figure 2.** Schematic representation of the testing setup for the IR camouflage tests: a,b) show the mechanism of the IR reflection and detection of the microfluidic surface in two states, non-activated (unfilled channels) and activated (channels filled with water).

UHMWPE-metalized layer-UHMWPE sandwich structure was cut by the craft cutter. For this cutting, the depth of the blade was precisely controlled so that only the top UHMWPE layer was cut without penetrating the metalized layer below. More information on the cutting settings could be found in Table S1 (Supporting Information). Next, the cut-out material inside the channel was removed. The top layer with the connection tubes was prepared as shown in Figure 1e–h. For the assembly of the two layers, the heat bonding temperature was lowered to 150 °C. Since the package bag itself is an ultra-thin multi-layered metalized sheet and the package bag tended to shrink due to polymer internal stress at temperatures above 150 °C. An image of the microfluidic device with an incorporated metalized sheet could be found in Figure S2 (Supporting Information).

## 2.6. Characterization

### 2.6.1. Microchannel Structure and Dimensions

The cross-section images of the microchannels with different dimensions were examined by field emission scanning electron microscopy (FE-SEM). The specimens were prepared by cutting the UHMWPE sheets with microchannels using stainless steel scissors. The microchannel samples were mounted on SEM

stubs with carbon tape and coated with a gold layer ( $\approx 2$  nm, Denton gold sputter) prior to SEM imaging.

### 2.6.2. Microfluidic Device Visible Camouflage Tests

The visible light camouflage tests were performed at the outdoor scenes of Edmonton, Canada during fall season (September and October 2022). Several most representative background colors were selected: green from grass, red from maple leaves and bricks, yellow from withered leaves, and brown from dirt. The visible camouflage of the prepared microfluidic devices was characterized using the canny edge-finding algorithm, which is a popular and effective technique to detect edges and is widely used in computer vision for object recognition and detection.<sup>[44–46]</sup> The working principle of the edge-finding algorithm involves the conversion of an image into a grayscale version, followed by the use of two thresholds to detect a large gradient magnitude. The gradient magnitude at each pixel was then compared to its neighbors. Given that the gradient magnitude represents the change in intensity at a particular pixel, the color-change edge could be precisely detected.<sup>[44–46]</sup> The complete MATLAB code could be found in the Supporting Information. The visible camouflage of the devices was also characterized by evaluating the color matching performance. Two comparison regions were selected on the microfluidic devices and the environmental background. Upon

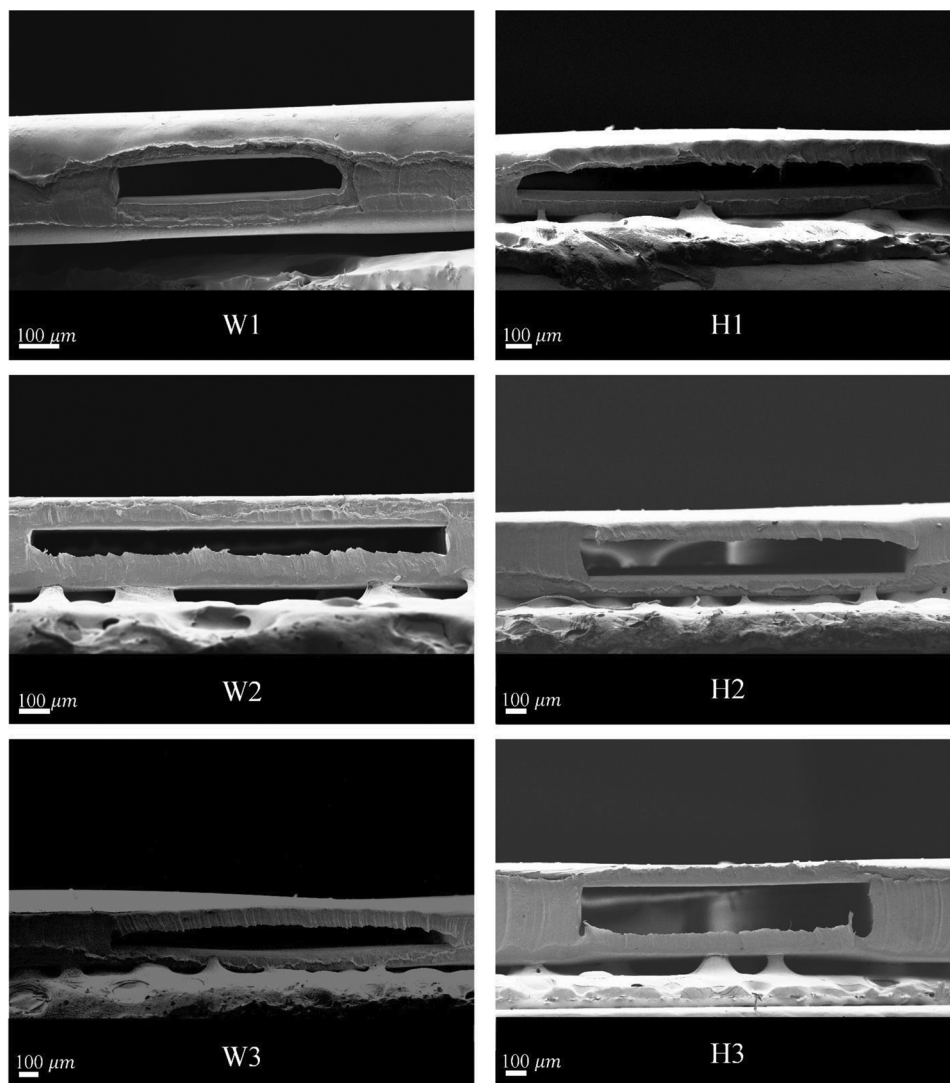


**Figure 3.** Cross-sectional SEM images for three different widths (W1, W2, and W3) and three different thicknesses (H1, H2, and H3) of the microfluidic device.

filling the dyed liquid, the average color of the unfilled device region, filled device region, and background region were evaluated in terms of RGB values, which is a standard color space coding.<sup>[47]</sup> The average color RGB codes within each region were assessed and compared to demonstrate the color matching performance. The complete MATLAB code could be found in the Supporting Information.

### 2.6.3. Microfluidic Device IR Camouflage Tests

The IR camouflage tests were performed indoors using a FLIR E95 camera to look at microfluidics that were heated or reflected a nearby thermal source. **Figure 2** shows a schematic of the testing setup for both states unfilled (**Figure 2a**) and filled (**Figure 2b**). The emitted IR radiation on the microfluidic device experienced absorption, transmission, and reflection (specular and diffusive) by the top layer of the microfluidic device. Reflection tests were

performed by exposing the microfluidic surface to a heat source (a 3D printer bed with a temperature of 100 °C) with an incident angle of 45° and placing the camera at a reflecting angle of 45°. The angle was chosen so that the infrared radiation from the heat source could be reflected by the metal layer embedded in the device. Images of the microfluidic devices were recorded using the IR camera at different liquid filling stages.

## 3. Results and Discussion

The cross-sectional FESEM images of W1, W2, W3, H1, H2, and H3 devices are shown in **Figure 3**. The desired/achieved channel widths of W1, W2, and W3 were 0.50/0.6, 1.0/1.3, and 2.0/1.8 mm, respectively, with a height of 100 μm ±9 μm. The desired/achieved channel heights of H1, H2, and H3 were 101.6/110.0, 203.2/184, and 304.8/264 μm, respectively. There was a slight deviation between the desired channel widths/heights and the values achieved. It was attributed to some

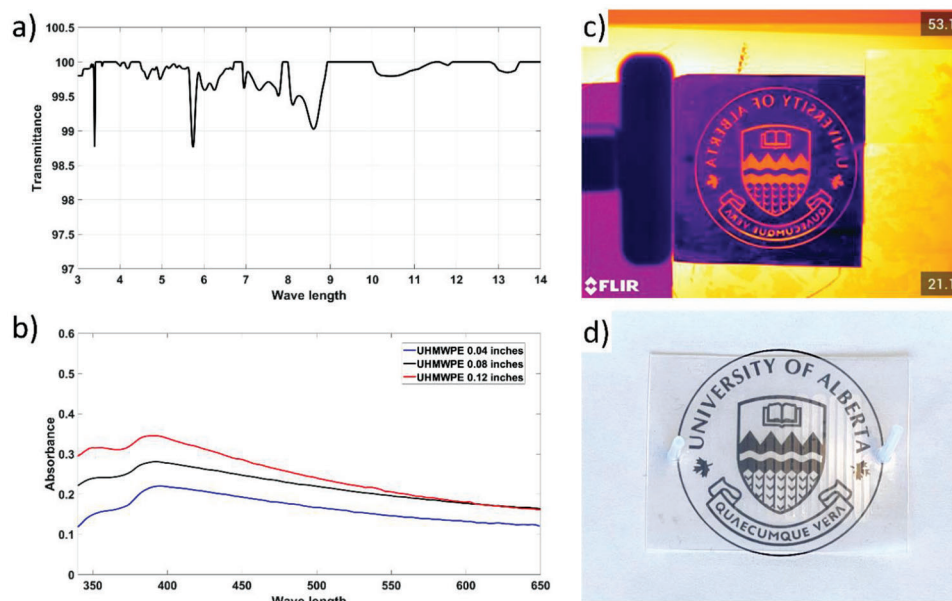


**Figure 4.** a) Transmittance results for an UHMWPE sheet with a thickness of 0.004 inches over the range of 3–14  $\mu\text{m}$ ; b) Absorbance results of UHMWPE sheets with different thicknesses (0.004, 0.08, and 0.12 inches); c) IR images of a microfluidic device (W1) placed in front of a metalized heated UofA logo; d) Microfluidic device (W1) placed on top of a printed UofA logo.

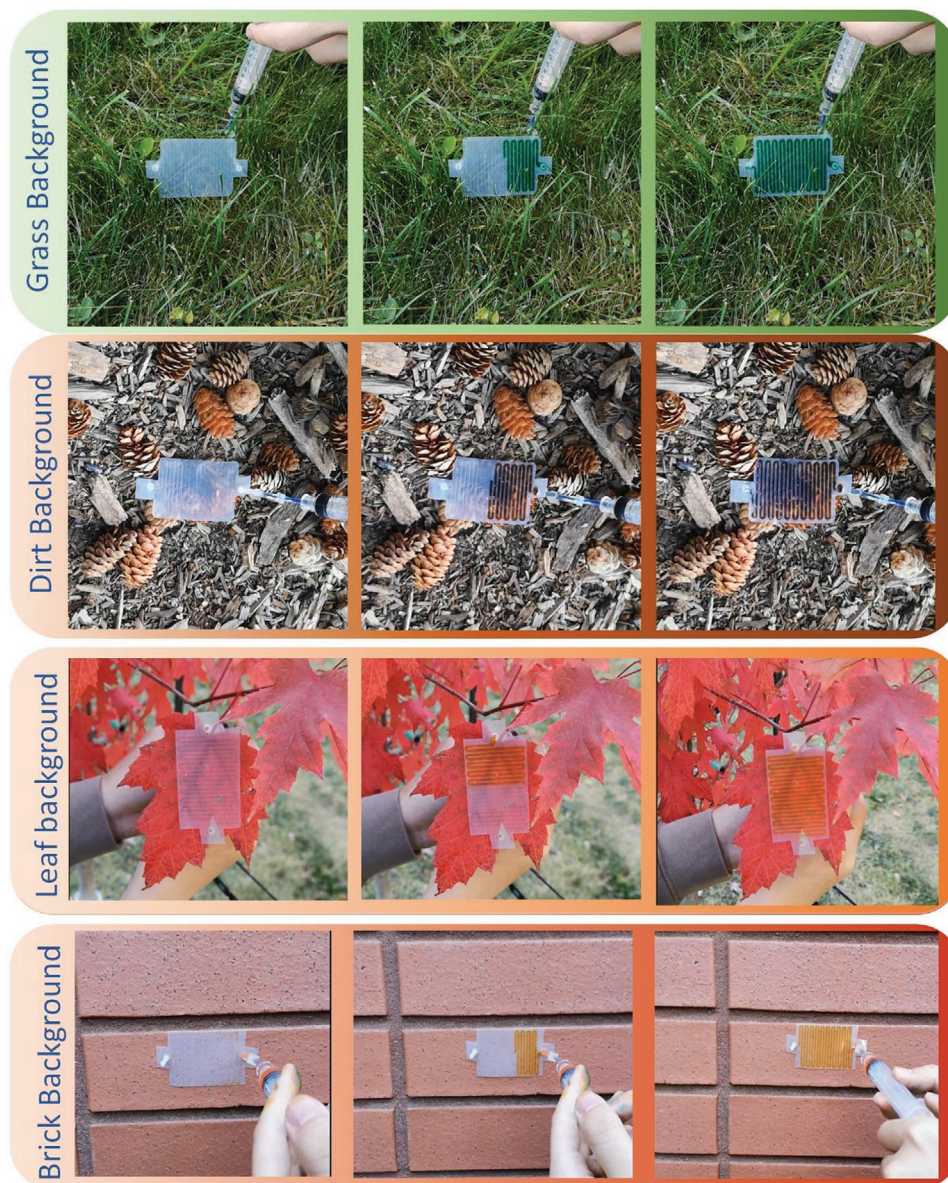
inconsistencies in the craft cutting step and rolling pressure during thermal bonding. Since H2 and H3 required thermal bonding of multiple UHMWPE layers, the difference between the desired and the achieved thickness was higher than for H1, indicating that rolling during thermal bonding has a significant effect on the height. Upon closer examination of the channel edges, as illustrated in Figure 3 (H3), it was observed that the edges were devoid of any inter-layer extension, suggesting a complete permanent bonding between the three UHMWPE layers.

Figure 4a,b show the FTIR and UV–vis transmittance and absorbance results for the UHMWPE sheets. Polyethylene is a semi-transparent material to infrared radiation because of the unique simplicity of its molecular structure.<sup>[48]</sup> It is made of a long chain of repeating units of ethylene monomers that are arranged such that there are relatively few chemical bonds that absorb/emit infrared radiation in the range of 3–14  $\mu\text{m}$ . Therefore, IR passes through the material to some extent, making it semi-transparent as shown in Figure 4a. The visible transparency of the UHMWPE comes from the interaction between the visible light and the polymer molecular structure. The photons of visible light do not have sufficient energy to excite the electrons in the PE molecules and cause them to absorb light. Therefore, visible light is transmitted through the material without being significantly absorbed (Figure 4b). Figure 4c shows a photograph of a microfluidic device placed on top of a heated University of Alberta (UofA) logo. The logo was made by cutting it from a metalized polyester film, which was then taped on top of a heated oven. The measured temperatures of the logo with and without the microfluidic device were 53 and 42  $^{\circ}\text{C}$ , respectively. As expected, there was a small drop in the apparent temperature due to the PE IR absorption. Figure 4d shows a picture of a microfluidic device placed on top of a UofA logo. Although the device consisted of two layers (0.008 inches in total) of PE, the UofA logo could be iden-

tified. In order to achieve higher transparency, a simple surface treatment was introduced. Figures S3 and S4 (Supporting Information) demonstrated the results of different surface treatment temperatures by heat-pressing a 100  $\mu\text{m}$  UHMWPE sheet between smooth surfaces such as Kapton tape on aluminum plates or polyester sheets. The treatment reduced the surface roughness and increased the visible transparency of the UHMWPE sheets. The visible appearance of the sheets changed from translucent to transparent.

The visible camouflage characterization considered the color differences between the environmental background and the microfluidic channels in both states (filled and unfilled) as shown in Figure 5. The microfluidic devices were placed in front of various backgrounds, such as grass, dirt, leaf, and brick, to demonstrate their camouflage capabilities. The unfilled devices were easily visible and distinguishable against the background, but as the devices were filled with dyed liquid, they quickly blended in with the surroundings and became hard to detect. By changing the color of the dye, the microfluidic devices were able to adapt to different backgrounds. The effectiveness of the device's camouflage was more pronounced for grass (Video S1, Supporting Information) and dirt (Video S2, Supporting Information) backgrounds, as there was a close match between the intensity of the dyed liquid and the background. However, in the case of the leaf and brick backgrounds, the match with the device color was still acceptable but not as good as in the former two scenarios. The intensity and color of the dyes are not limited to what was used in this study and can be adjusted and modified as required. Therefore, adjusting the color and intensity of the dyed liquid can result in devices that are optimized for specific environmental conditions, therefore increasing their effectiveness in the field. The total time for the device actuation was typically <15 s; it was controllable by the change in the pressure





**Figure 5.** Images of microfluidic devices tested for their camouflage capabilities with different backgrounds (grass, dirt, leaf, and brick). The photos were captured in outdoor conditions on the University of Alberta campus.

applied to the syringe. With a larger pressure, the color changing was faster. By retracting the dyed liquid, the microfluidic device was able to return to a semi-transparent appearance. It is worth mentioning that our developed method for the permanent interface between macro-scale PE tubes and micro-scale channels ensured having robust and leak-free operations. All the prepared devices exhibited airtight and watertight features providing a strong and reliable seal that can withstand the high pressures and flows typically encountered in microfluidic.

The aim of visible camouflage is to conceal an object or individual when observed under visible light conditions.<sup>[49]</sup> This is achieved by reducing or eliminating the contrast between the object and the background, and by disguising the object's edges. Typically, this involves using colors and patterns that are simi-

lar to those found in the surrounding environment or by incorporating contrasting colors to break up the object's outline. To achieve effective concealment, it is necessary for camouflage devices to incorporate multiple colors, as natural environments are not comprised of a single color. Fortunately, our devices can easily be fabricated as a multi-input/output system to blend in multicolored background. Moreover, our fabrication process could easily be adjusted to fabricate devices with different channel patterns and shapes. By carefully designing the channel dimensions, the channel coverage ratio can be maximized with the rest of the surface areas – including channel walls and device edges – minimized. The minimum feature size of walls and channels for the equipment and materials used is  $\approx 300$   $\mu\text{m}$ . **Figure 6** shows three devices that are connected to correspond to distinct military



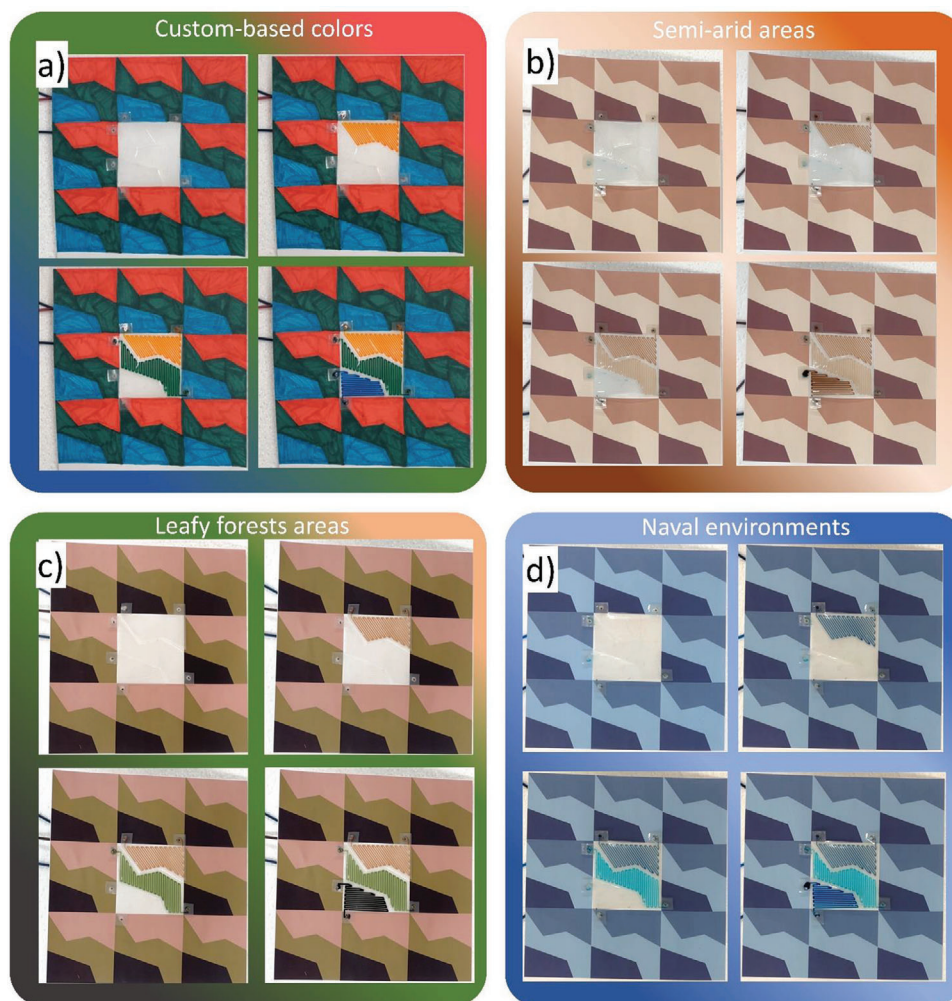


**Figure 6.** a–d) Multi-input/output microfluidic devices for visible camouflage capabilities in multicolored backgrounds; The devices were tailored to match the colors and patterns of semi-arid climates (Middle East & Asia), leafy forests (North America & Europe), and naval environments.

camouflage patterns commonly utilized in various environmental conditions (Videos S3 and S4, Supporting Information). These patterns were tailored to match the requirements of semi-arid climates (Middle East & Asia), leafy forests (North America & Europe), and naval environments.<sup>[17,49]</sup> The multi-input/output microfluidic device demonstrated high matching capability in these diverse environments, making it a versatile and adaptable solution for visible camouflage. Notably, the device was not limited to a specific pattern, allowing it to be used across a wide range of environmental conditions. By providing a universal camouflage solution, this device could eliminate the need for multiple garments to match specific environments.

To gain a deeper understanding of the visible camouflage effects of the microfluidic devices, further analysis was conducted using the canny edge finding algorithm. This algorithm is a commonly used image processing technique that can identify the edges of objects in an image.<sup>[46]</sup> By applying this algorithm to images of the devices in various environmental settings, we assessed the effectiveness of the camouflage in terms of its ability to disguise or break up the outline of the device. The unfilled mi-

crofluidic devices showed up as black voids and were thus very distinguishable and detectable by the edge-finding algorithm. Interestingly, the filled devices merged into the background and were not recognizable. These results confirmed that the microfluidic devices were successful in reducing the contrast between the device and the background, as well as disguising the edges of the device. Results for the leaf and brick backgrounds can be found in the Supporting Information (Figure S5, Supporting Information). **Figure 7.**

Besides disguising the edges and matching the shapes of the microfluidic device, the match of colors is also vital for camouflage evaluation. We assessed the color-matching performance upon filling the channels by evaluating the average RGB color values of the microfluidic device and the background. The results are presented in **Figure 8**, where the first and second columns demonstrate the labeled environmental backgrounds and microfluidic devices in both states (filled and unfilled). The red square represents the selected background region, while the green square represents the selected microfluidic device region. The third column presents the analysis results of the average

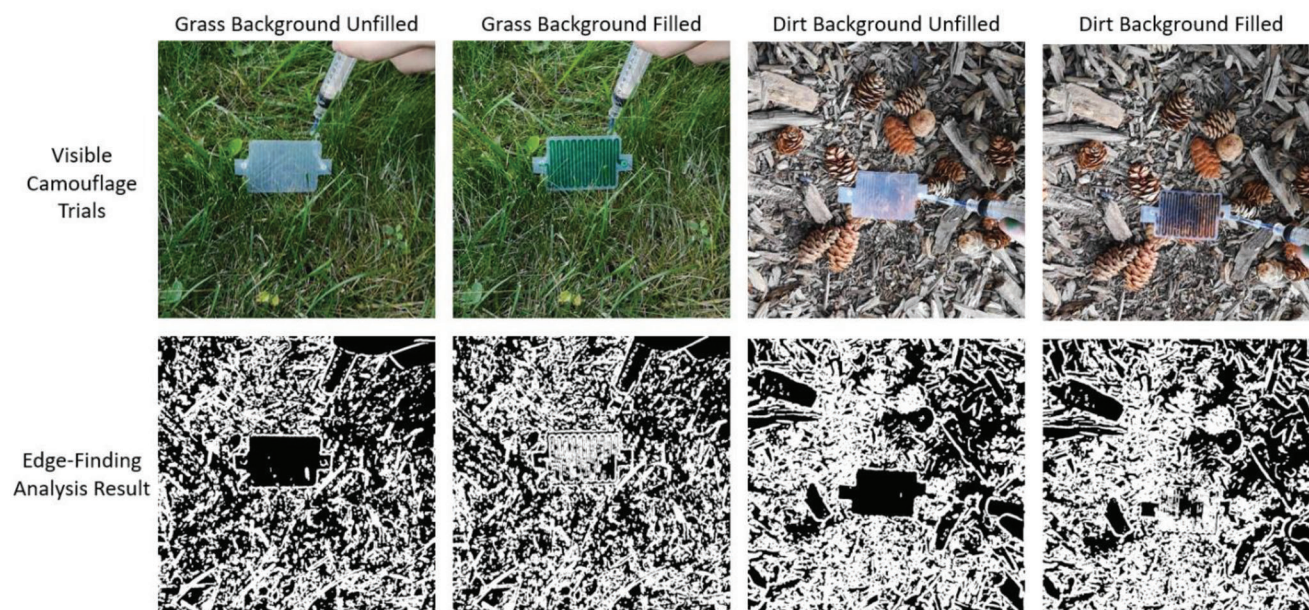


**Figure 7.** Canny edge-finding algorithm analysis results for selected trials (grass and dirt background). The first row provides images of the unfilled and dye-filled devices against the background. The second row is the results from MATLAB of “Canny” edge finding algorithm. The white lines shows the edges detected by the code; the empty channels for both grass background and dirt background do not have detected edges inside. Some edges showed inside are most likely due to objects in front of the device. As for the filled channels, there are many detected edges inside the region of the device, which blurred the actual boundary between the device and background.

color RGB values for the unfilled device region, filled device region, and background region. The bar charts separately display the red, green, and blue values to show the matching trend as the device is filled. RGB codes have a range of [0–255], where 0 represents black, and if all three R, G, and B values are at their maximum of 255, it appears as white. Under normal conditions, the unfilled device appears visibly translucent (whitish), thus the RGB codes for the unfilled device have relatively high values. As shown in Figure 8, filling the device results its RGB values to have a significant trend of matching to the background RGB values. The RGB values of the filled devices and background are similar, indicating a similar color. These results support the successful matching of the microfluidic devices with the background color. The detailed RGB values can be found in the Supporting Information.

IR camouflage is another important application that can be achieved using a modified version of this microfluidic device. In general, smooth surface metals have low emittance but high infrared reflectivity.<sup>[50–52]</sup> This makes metal object thermally visible as long as there is a heat source in the region even the metal object itself does not emit much infrared radiation. The reflection from the heat source makes metal appear to be at a higher temperature. However, this reflected IR radiation can be easily blocked by a thin layer of water. By circulating a layer of water above the reflective metal layer, the IR reflection can be blocked, which makes the metal appear colder (ambient temperature). This allows the manipulation of the IR appearance of metals. Versions of W1, W2, and W3 devices were modified by embedding a metal surface between the channels and the bottom layer. The result of the measurement of their IR appearance was presented in Figure 9.

The first column in Figure 9 shows the empty channel’s IR reflection appearance against a hot 3D printer bed (surface temperature at 100 °C); the second column shows the reflection appearance from the filled channel with DI water; and the third column shows the measured average temperatures data of the metal surface by the IR camera for both filled and unfilled channels. The area of measurement was indicated in each subfigure in column 1 and column 2 as a white square. The measured average temperature results for the unfilled W1, W2, and W3 devices were 45.3, 45.4, and 46.7 °C, respectively. Although the temperature of the heated source was set at 100 °C, the highest average reflected temperature was 46.7 °C. This could be attributed to the presence of UHMWPE layers above the metal surface. Despite the high IR transparency of the PE sheet, it still absorbed a certain portion of the IR radiation before it reaches the underlying metal surface. Furthermore, after the IR radiation is reflected from the metal, the PE sheet continued to absorb a fraction of it. As the IR radiation passed twice through the PE sheet before it was detected by the IR camera, it significantly contributed to the observed temperature difference. Another possible factor could be the precision of the IR camera. This type of camera measures the average temperature within a measurement zone rather than the temperature at a specific point. Upon filling the devices with DI water, the area average temperatures of W1, W2, and W3 were 40.1, 37.4, and 36.0 °C, respectively. The area average temperature drop of all devices was 8.3 °C, demonstrating the effectiveness of our method in blocking reflected IR radiations. Notably, while the area average temperature drop was lower than 9 °C, the spot temperature at the channel dropped from 50.1 to 31.6 °C upon filling, which was  $\approx 19$  °C decrease. In addition, the width of the channels had



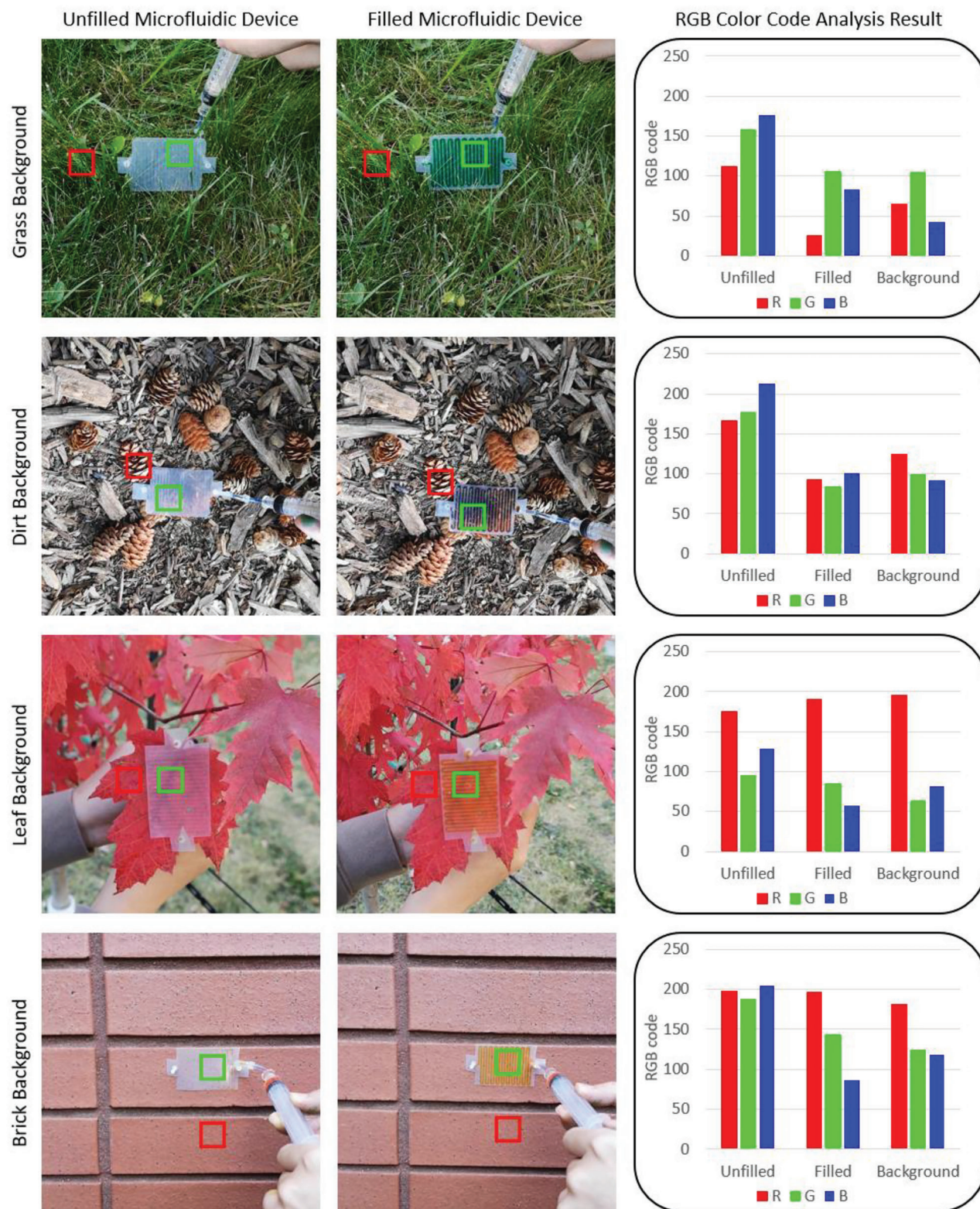


**Figure 8.** Average color RGB codes analysis results for different backgrounds (grass, dirt, leaf, and brick). The first and second columns presented the labeled images to indicate the regions. Red squares are the environmental background regions and green squares are the device regions. The results were presented in the third column, which included all the RGB values for the unfilled device region, filled device region, and background region. The filled device region has very similar RGB values as the background region comparing to an unfilled device, which indicated the color matching was successful.



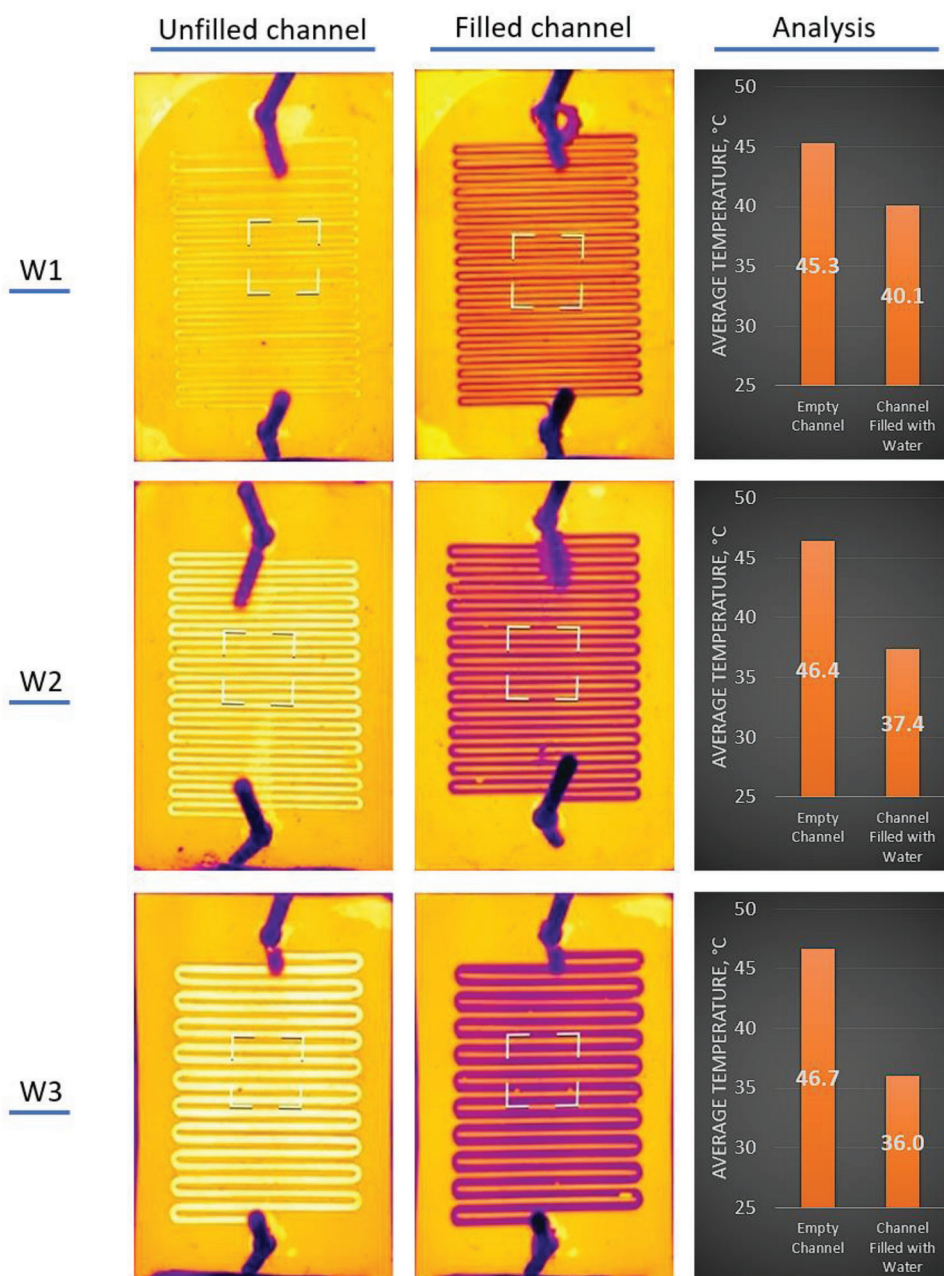


**Figure 9.** Images of the IR reflection appearance of W1, W2, and W3 positioned in front of a hot 3D printer bed (100 °C) under unfilled (column 1) and filled (column 2) states. The average temperature measurement area was indicated in each subfigure in column 1 and column 2 as the white square. Column 3 shows the area average temperature drop upon filling the microfluidic devices with DI water.

an obvious impact on the reflected IR appearance, with wider channels appearing as colder surfaces. This was primarily due to the large channel area versus support wall structure that was achieved for these designs and suggests future improvements are possible.

#### 4. Conclusion

In this work, we fabricated and characterized microfluidic devices made entirely from polyethylene (UHMWPE) including

inlet/outlet tubes (PE). The devices are inexpensive (<0.09 CAD per piece), extremely durable, and relatively transparent to both visible light and thermal infrared wavelengths. The fabrication technique is simple and relies solely on xurography and thermal bonding. The fabrication of the microfluidic device is fast (a few minutes per piece), and thanks to the simplicity of the process, it would be possible to mass produce this type of microfluidic device. Our characterization showed the channel was watertight and airtight, which demonstrated the reliability of the device. Besides the unique fabrication process, our group developed

some innovative applications of this microfluidic device with microchannels. Due to the transparency of polyethylene, it has been shown that this microfluidic device is capable of achieving visible camouflage by circulating a dyed liquid through the microchannel. A prototype has been fabricated to demonstrate the ability to have multiple camouflage colors on the same device. IR camouflage was achieved by slightly modifying the original structure of the microfluidic device. An ultra-thin metalized polyethylene was added between the microchannel layer and the bottom layer. IR reflection tests showed the capability to manipulate the IR reflectivity of metals and therefore the apparent temperature of the system, without altering its actual temperature. Improved thermal infrared performance should be achievable using thinner polyethylene sheets. The low cost, durability, and ease of fabrication of these microfluidic devices, combined with their unique camouflage properties, make them promising candidates for a wide range of applications, including environmental monitoring, medical diagnostics, and military and surveillance operations. The ability to mass produce these devices with minimal resources could lead to significant advancements in these fields and contribute to the development of more accessible and affordable technologies.

## Supporting Information

Supporting Information is available from the Wiley Online Library or from the author.

## Acknowledgements

This research was funded by the Department of National Defence (DND) of Canada program Innovation for Defence Excellence and Security (IDEaS) under Project W7714 228051/001/SV1.

## Conflict of Interest

The authors declare no conflict of interest.

## Data Availability Statement

The data that support the findings of this study are available from the corresponding author upon reasonable request.

## Keywords

adaptive infrared camouflages, adaptive visible camouflages, flexible microfluidic devices, microfluidic devices, polyethylene

Received: May 12, 2023  
Revised: July 8, 2023  
Published online: August 25, 2023

- [3] A.-G. Niculescu, C. Chircov, A. C. Bîrcă, A. M. Grumezescu, *Int. J. Mol. Sci.* **2021**, 22, 2011.
- [4] S. C. Terry, J. H. Jerman, J. B. Angell, *IEEE Trans. Electron Devices* **1979**, 26, 1880.
- [5] K. E. Petersen, *IEEE Trans. Electron Devices* **1979**, 26, 1918.
- [6] F. C. M. Van De Pol, J. Branebjerg, in *Micro System Technologies 90*, (Eds. H. Reichl), Springer, Berlin Heidelberg **1990**, pp. 799–805.
- [7] D. Erickson, D. Li, *Anal. Chim. Acta* **2004**, 507, 11.
- [8] A. Manz, N. Graber, H. M. Widmer, *Sens. Actuators B Chem* **1990**, 1, 244.
- [9] B. Kuswandi, Nuriman, J. Huskens, W. Verboom, *Anal. Chim. Acta* **1990**, 601, 141.
- [10] P. Cui, S. Wang, *J. Pharm. Anal.* **2019**, 9, 238.
- [11] G. Weisgrab, A. Ovsianikov, P. F. Costa, *Adv. Mater. Technol* **2019**, 4, 1900275.
- [12] M. Stevens, S. Merilaita, *Philos. Trans. R. Soc. B Biol. Sci.* **2009**, 364, 423.
- [13] M. Stevens, I. C. Cuthill, A. M. M. Windsor, H. J. Walker, *Proc. R. Soc. B Biol. Sci.* **2006**, 273, 2433.
- [14] R. Hanlon, *Curr. Biol.* **2007**, 17, R400.
- [15] M. Stevens, S. Merilaita, *Animal Camouflage: Mechanisms Function*, Cambridge University Press, Cambridge **2011**.
- [16] C. J. Lin, Y. T. Prasetyo, N. D. Siswanto, B. C. Jiang, *Color Res. Appl.* **2019**, 44, 367.
- [17] L. Talas, R. J. Baddeley, I. C. Cuthill, *Philos. Trans. R. Soc. B Biol. Sci.* **2017**, 372, 20160351.
- [18] M. Friškovec, H. Gabrijelčič, *Fibres Text. East. Eur.* **2010**, 18, 81.
- [19] A. King, *Millennium* **2014**, 42, 397.
- [20] X. Wei, G. Li, K. Wang, *IEEE Access* **2021**, 9, 67559.
- [21] F. Steffens, S. E. Gralha, I. L. S. Ferreira, F. R. Oliveira, *Key Eng. Mater.* **2019**, 812, 120.
- [22] L. M. Degenstein, D. Sameoto, J. D. Hogan, A. Asad, P. I. Dolez, *Micromachines* **2021**, 12, 773.
- [23] M. Zhang, S. Li, *SpringerPlus* **2016**, 5, 580.
- [24] C. Feng, M. Mao, X. Zhang, Y. Liao, X. Xiao, H. Liu, K. Liu, *Microsyst. Nanoeng.* **2023**, 9, 43.
- [25] S. A. Morin, R. F. Shepherd, S. W. Kwok, A. A. Stokes, A. Nemiroski, G. M. Whitesides, *Science* **2012**, 337, 828.
- [26] M. Zhang, S. Li, *J. Exp. Nanosci.* **2018**, 13, 221.
- [27] L. Li, H. Li, S. Li, in 2022 IEEE International Conference on Electrical Engineering, Big Data Algorithms (EEBDA), **2022**, 303, 307.
- [28] K. Raj M, S. Chakraborty, *J. Appl. Polym. Sci.* **2020**, 137, 48958.
- [29] J. C. McDonald, G. M. Whitesides, *Acc. Chem. Res.* **2002**, 35, 491.
- [30] J. C. McDonald, D. C. Duffy, J. R. Anderson, D. T. Chiu, H. Wu, O. J. A. Schueller, G. M. Whitesides, *Electrophoresis* **2000**, 21, 27.
- [31] C. Hu, S. Lin, W. Li, H. Sun, Y. Chen, C.-W. Chan, C.-H. Leung, D. L. Ma, H. Wu, K. Ren, *Lab Chip* **2016**, 16, 3909.
- [32] K. Kobayashi, H. Onoe, *Microsyst. Nanoeng.* **2018**, 4, 17.
- [33] E. Team, Elveflow, <https://www.elveflow.com/microfluidic-reviews/general-microfluidics/the-polydimethylsiloxane-pdms-and-microfluidics/>, (accessed: December 2022).
- [34] E. Roy, M. Geissler, J.-C. Galas, T. Veres, *Microfluid. Nanofluidics* **2011**, 11, 235.
- [35] S. M. Scott, Z. Ali, *Micromachines* **2021**, 12, 319.
- [36] X. Hou, Y. S. Zhang, G. T.-D. Santiago, M. M. Alvarez, J. Ribas, S. J. Jonas, P. S. Weiss, A. M. Andrews, J. Aizenberg, A. Khademhosseini, *Nat. Rev. Mater.* **2017**, 2, 17016.
- [37] A. Waldbaur, H. Rapp, K. Länge, B. E. Rapp, *Anal. Methods* **2011**, 3, 2681.
- [38] J. Hwang, Y. H. Cho, M. S. Park, B. H. Kim, *Int. J. Precis. Eng. Manuf.* **2019**, 20, 479.
- [39] D. I. Walsh, D. S. Kong, S. K. Murthy, P. A. Carr, *Trends Biotechnol.* **2017**, 35, 383.

[1] G. M. Whitesides, *Nature* **2006**, 442, 368.

[2] K. Ren, J. Zhou, H. Wu, *Acc. Chem. Res.* **2013**, 46, 2396.

- [40] D. A. Bartholomeusz, R. W. Boutte, J. D. Andrade, *J. Microelectromechanical Syst.* **2005**, 14, 1364.
- [41] M. Islam, R. Natu, R. Martinez-Duarte, *Microfluid. Nanofluidics* **2015**, 19, 973.
- [42] C. K. Fredrickson, Z. Hugh Fan, *Lab Chip* **2004**, 4, 526.
- [43] Y. Temiz, R. D. Lovchik, G. V. Kaigala, E. Delamarche, *Microelectron. Eng.* **2015**, 132, 156.
- [44] J. Canny, *IEEE Trans. Pattern Anal. Mach. Intell.* **1986**, PAMI-8, 679.
- [45] L. Ding, A. Goshtasby, *Pattern Recognit* **2001**, 34, 721.
- [46] Y. Luo, R. Duraiswami, in 2008 IEEE Computer Society Conference on Computer Vision Pattern Recognition Workshops, **2008**, 1, 8.
- [47] S. Süssstrunk, R. Buckley, S. Swen, in Proc. IS&T/SID 7th Color Imaging Conference, **1999**, 127–134.
- [48] M. Chen, D. Pang, H. Yan, *iScience* **2022**, 25, 104726.
- [49] R. J. Denning, in *Engineering of High-Performance Textiles*, (Eds. M. Miao, J. H. Xin), Woodhead Publishing, Cambridge **2018**, pp. 349–375.
- [50] W. Przybył, W. Radosz, A. Januszko, *Color. Technol.* **2020**, 136, 407.
- [51] M. Kobayashi, A. Ono, M. Otsuki, H. Sakate, F. Sakuma, *Int. J. Thermophys.* **1999**, 20, 299.
- [52] C. Hu, Jian Liu, J. Wang, Z. Gu, C. Li, Q. Li, Y. Li, S. Zhang, C. Bi, X. Fan, W. Zheng, *Light Sci. Appl.* **2018**, 7, 17175.